Dynamics of a pre-stalled windturbine blade using control of circulation at the trailing-edge

V. Jaunet, C. Braud and T. Piquet

LHEEA laboratory, 1 rue de la Noe, 44321 Nantes, FRANCE . vincent.jaunet@ec-nantes.fr

Abstract :

Windturbines evolves in the atmospheric boundary layer at a height where strong wind velocity fluctuations in both amplitude and direction can be found. These fluctuations create undesirable mechanical loads on the turbine that can lead to severe damages. We study the possibility of controlling these unsteady loads by mean of fluidic actuation on the trailing edge of a modified windturbine profile. The dynamics of the system, i.e. *lift gain and response time, is investigated using step responses of the chordwise pressure distribution.*

Key Words : Windturbine, Lift control, fluidic actuation

1 Introduction

Windturbines evolves in the atmospheric boundary layer at a height where strong wind velocity fluctuations in both amplitude and direction can be found (Kaimal et al., 1972). These fluctuations modify the actual forces acting on the blade and therefore create undesirable mechanical loads on the turbine that can lead to severe damages to the turbine.

Closed-loop control of the blade lift might be considered to reduce or even alleviate these mechanical loads. Closed loop lift control of airfoils has been of great interest especially for post-stall performance recovery. Williams et al. (2009, 2010) used leading edge actuation to recover lift on a 3D airfoil after separation of the boundary layer. Colonius and Williams (2011) puts forward that the dynamics response of lift shows some universal features, whatever the actuation or the type of profile of interest (Woo et al., 2008; Williams et al., 2010). They measured a response time of about a ten of chord time $t^* = C/U_\infty$, where C is the chord and U_∞ is the freestream velocity. The same order of magnitude is also observed for detached flows over more canonical configurations (Darabi and Wygnanski, 2004a,b; Mathis et al., 2009; Shaqarin et al., 2013). On top of that, it is generally observed that a pulsed fluidic actuation has increased performances compared to a continuous fluidic actuation (Jones et al., 2002; Shaqarin et al., 2013). Initial vorticity when the jet is blown might explain the extra suction obtained by pulsed jets. Similar to the observation of initial lift gain of controlled stalled airfoils (Colonius and Williams, 2011). It seems that the research effort in closed-loop lift control has mainly been focused on post-stall lift recovery.

Recently Troshin and Seifert (2013) performed closed-loop lift control on an airfoil with distributed fluidic actuation on the suction side of an unstalled thick wing, aiming at the recovery of lift loss due to surface degradation. They observed the lift to respond as a second order system with a typical response time of 8.1 chord time (*i.e.* in the same order of magnitude of the stalled cases). They also showed

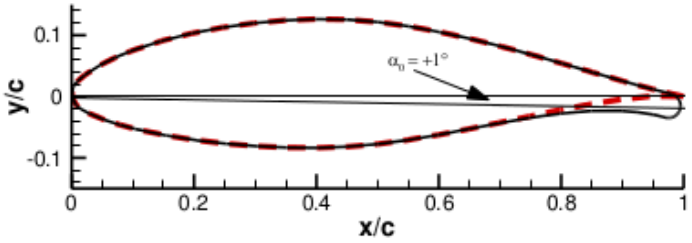

FIGURE 1 – The original $NACA-65_4421$ airfoil is in red dotted lines and the control profile $NACA-65_4421-CC$, used in this study, is in solid black line.

that the system dynamics may vary with both the Reynolds number and the angle of attack (AOA). The gain gets higher as the AoA increases and the response time gets faster as the AoA and/or the Reynolds number increases. On the other hand, circulation control at the trailing is a widely used technique for lift enhancement in pre-stall configurations. Since the early work of Englar (1972); Englar and Williams (1971); Englar (1975) circulation control using secondary injection and Coanda effect at the trailing edge is known to produce an efficient way of modifying the lift of a wing profile. The lift gain produced by Coanda jet circulation control is obtained through a displacement of the forward and aft stagnation points, hence changing the circulation around the wing (Englar, 1975), but also through the very low wall pressure that the Coanda turning can produce on the Coanda surface (Kadosch, 1958). Circulation control has been investigated for a great variety of field from helicopter blades to propellers, showing the great interest of the research community in such techniques (Kweder et al., 2010). Circulation control has only recently been investigated in the field of windturbine aerodynamics (Dumitrache et al., 2012; Shires and Kourkoulis, 2013; Baleriola et al., 2016; Leroy et al., 2016; Braud and Guilmineau, 2016). Cagle and Jones (2002) and Jones et al. (2002) provided feasibility evidence of CC on wing profiles similar to the one used on windturbines but only gave steady-state information on the system. Hence, to the authors knowledge, few studies aimed at revealing the dynamics of circulation control systems.
The aim of this paper is to provide steady-state as well a dynamical information of a pre-stalled wind-turbine blade profile whose trailing edge is modified to allow circulation control by means of spanwise distributed discrete microjets. The control objective is to compensate atmospheric perturbations from manipulation of the lift. The experimental apparatus is described in the section II. In section III and IV, we provide respectively, the steady and dynamic responses of the system perturbed by a control action step. Concluding remarks are given in section V.

2 Experimental set-up

2.1 Blade profile

The trailing edge of a $NACA-65_4421$ airfoil profile has been rounded (radius of curvature 2%) and the camber of the airfoil has been adjusted to compensate aerodynamic degradation due to the round trailing edge. The profile is presented in figure 1.

The discrete microjets are distributed along the wing span from the stack of thin profiles (1 mm) and thick blind profiles (20mm). The thin profiles possess a round hole connected to a small air circuit (of 1 mm width) open to the surface of the profile. This is illustrated in figure 2 (Left). The thick profile

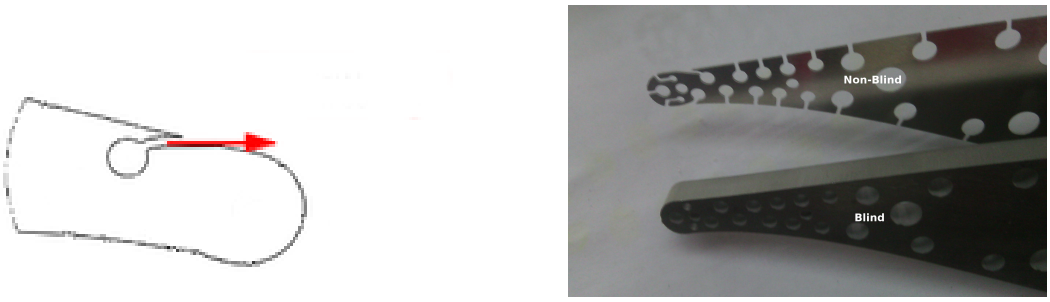

FIGURE 2 – Left : diagram of a thin (non-blind) profile. Right :photograph of the thick (blind) and thin (non-blind) profiles.

possess the same round hole with no connection to the surface. Once stacked, the holes form a plenum chamber in the span direction of the profile, which can be connected to pressurized air to generate discrete squared fluidic microjets. The same principle was used to measure pressure around the chord, so that the pressure is integrated along the span of the profile, very close to what can be obtain in a 2D pressure field. One can see figure 2 (Right) for samples of thin (non-blind) and thick (blind) profiles.

2.2 Windtunnel

The measurements were conducted at the University of Orléans, in the Lucien Malavard closed return wind tunnel of the PRISME laboratory. It has a section test of 5 m long with a cross- section of 2 m x 2 m. The turbulence level in this test section is below 0.4%. In the present study, the operating speed of the wind tunnel was $U_\infty = 10m/s$. The 2D blade was mounted between two vertical flat planes in order to achieve a 2D flow configuration. At this free stream velocity the Reynolds number of the flow based on the chord length is slightly above 2×10^5.

2.3 Air delivery system

The compressed air circuit is composed of a pressure regulator, a plenum tank and the actuation is monitored through the help of electric valves. The pressure regulator helps is used to control the actuation intensity which is set prior to the experiment. The intermediate plenum tank ensures the stability of the actuators stagnation pressure while the flow is rapidly set with the valves. An electro-pneumatic time delay of opening was measured at $0.014\ s$ very fast compared to the flow time scales, expected to be of the order of the several chord convective time $C/U_\infty = 0.03\ s$ (Colonius and Williams, 2011).
The momentum coefficient C_μ is used as a measure of the actuation strength. It is defined as :

$$C_\mu = \frac{Q_{\mu j} V_{\mu j}}{1/2 \rho_\infty U_\infty^2 S_{ref}}, \tag{1}$$

where, $Q_{\mu j}$ is the injection mass flow rate, $V_{\mu j}$ is the injected flow velocity and the subscript ∞ refers to the external flow conditions. It is straightforward to show that :

$$C_\mu = 2 \cdot \frac{P_{\mu j} M_{\mu j}^2}{P_\infty M_\infty^2} \cdot \frac{S}{S_{ref}}, \tag{2}$$

where $P_{\mu j}$ is the static pressure of the micro-jet at the exit section and $M_{\mu j}$ is the exit Mach number of the micro-jet. As long as the injection stays subsonic — *i.e. the ratio of stagnation to static pressure stays below the* $M = 1$ *level :* $P_{0\mu j}/P_{ext} < 1.89$ —, $P_{\mu j}$ is equal to the external pressure at the location of the

actuator. Hence, at constant incoming conditions and fixed actuator position, $P_{\mu j}/P_\infty$ only depends on the AOA. Therefore, for subsonic injection and fixed geometry, C_μ depends on the ratio of micro-jet to external Mach numbers $M_{\mu j}/M_\infty$, which can only be changed by increasing the stagnation pressure of the micro-jet. The relationship between C_μ and the stagnation pressure of the micro-jets is theoretically non-linear, but in the limited range of $M_{\mu j}$ that could be set in the present experiment C_μ can be well approximated by an linear function.
Note that we used the compressible form of the C_μ because the micro-jet Mach number can easily exceed $M_{\mu j} = 0.3$ Jones et al. (2002) (the respective stagnation to static pressure ratio is 1.064). Furthermore, since $M_{\mu j}$ is directly obtained from $P_{0\mu j}/P_{\mu j} = (1 + \frac{\gamma-1}{2}M_{\mu j}^2)^{\frac{-\gamma}{\gamma-1}}$, there is no need to know the temperature of the micro-jet flow, which makes this formulation easier to use.
The experimental set-up allowed to vary the C_μ in the $[0 - 0.14]$ range.

2.4 Measurement apparatus

2.4.1 Balance

First, the profile was placed on a 6-axis balance system to measure the time averaged lift and drag. The balance was carefully calibrated so that lift and drag uncertainties were estimated to be less than 2% in the free stream velocity range used in this study.

2.4.2 Wall pressure sensing

The pressure taps were connected to two *Chell MicroDAQ* pressure scanners to synchronously obtain the pressure field around the profile. The scanners were externally triggered at 500Hz, the maximum possible sampling frequency with this configuration. At each rising edge of the trigger signal, the pressure scanner performed an acquisition of all the channels and sent the digital values over the network to a dedicated computer. The number of received samples were compared to the number of rising edges to validate the acquisition.

2.4.3 Synchronization

Given the numerous different measurements that had to be performed synchronously, a dedicated triggering device was designed. The pressure sampling and the actuation systems were generated using the internal timers and pulse width modulation capabilities of an Atmel atmega2560 microcontroler. In the meantime, the trigger and pressure signals were recorded on an independent ADC system to *a posteriori* be able to perform all the desired time dependent analysis.

3 Steady response

3.1 Aerodynamic performances

In figure 3 we present a comparison of the lift curves for different actuation intensities (*i.e* C_μ). The unmanipulated lift curve shows the expected trends for this kind of profiles : a linear lift relation with the AOA for $\alpha < 9$, followed by a saturation for higher AOA corresponding to the boundary layer separation from the upper surface of the blade. From this figure, we can see that the actuation has numerous effects on the lift curves. First of all, as expected from previous circulation control attempt, the lift is increased

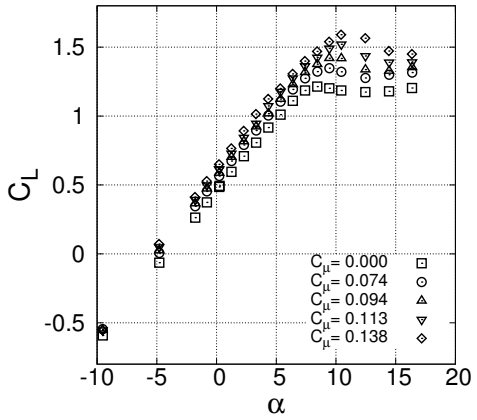

FIGURE 3 – Comparison of actuated versus non-actuated lift curves for the current wing $U_\infty = 10m/s$

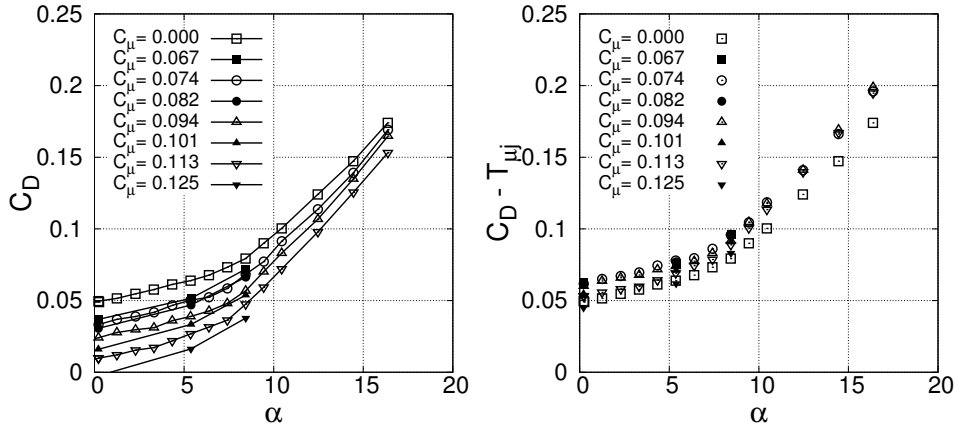

FIGURE 4 – Comparison of actuated versus non-actuated drag curves for the current blade profile (left). Drag compensated using control jet thrusts (right)

for all angle of attack (Seifert et al., 1993; Jones et al., 2002). With control, the lift curve is displaced towards the higher lift values. This is an important characteristic if one aims at compensating the lift changes due to external wind gusts for example. It is also clear from the C_L curve that the actuation plays a significant role in delaying the stalled regime of the airfoil.

In figure 4 (left) we present a comparison of the C_D curves for different C_μ. At a first glance, one could think that the control decreases the drag of the profiles. However, this is a simple micro-jet thrust effect. Indeed, each individual micro-jet acts as a small nozzle that creates thrust in the opposite direction of drag that can be measured with zero free stream velocity. By removing this thrust effect on the drag measurements, drag curves overlap for all controlled cases, pointing that there is no tremendous effect of the actuation on the profile drag (see figure 4 right).

3.2 Steady state gains

We plot in figure 5 the lift coefficient gain against C_μ for various AOA in the attached regime and thus the input/output steady state gains for different states of the system. It is clear that the control gives a linear change in lift for all presented AOA. As stated earlier, the relationship between the micro-jet stagnation pressure and C_μ can be well approximated by a linear relation. Since the relation between C_μ

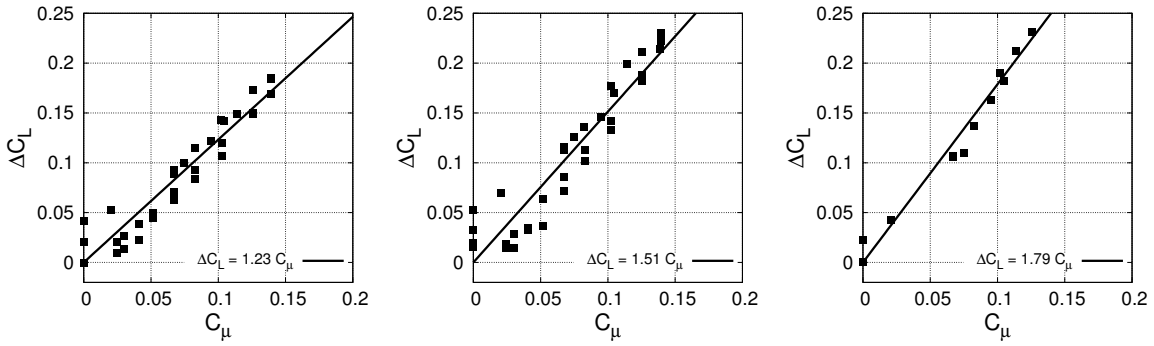

FIGURE 5 – Lift coefficient as function of injection coefficient for $\alpha = 0$ (left), $\alpha = 5$ (center), $\alpha = 8$ (right).

and the micro-jet generating pressure is almost linear (see dedicated previous section), it means that the lift increment due to the actuation is directly proportional to the pressure set in the micro-jet stagnation chamber. This is an interesting consideration for a future feedback control strategy because pressure is a quantity easily measured.

We present on the same figures linear regressions of the measured lift increments. It can be seen that the regression easily captures the trends. The observable scatter is a simple cause of the lift measurement uncertainty at this flow velocity. We see, from the linear regression slope coefficient indicated in the figure legends, that the actuation efficiency is greater for higher angle of attack. Therefore, the input/output relationship of the system (i.e. pre-stall blade profile lift) is linear with a steady state gain, but with a proportionality coefficient that varies with the state of the flow through, at least, modification of the AOA.

4 Dynamic response

In this section we study both the wall pressure step response and the subsequent lift response at the zero degree of AOA.

4.1 Chordwise pressure

Figures 6 show pressure responses to a step in actuation, measured at different locations along the chord, on the wing upper side. These step responses where obtained by averaging 300 different uncorrelated realizations. The measured pressure show a different dynamic response depending on its location on the chord. Fastest responses (i.e. lowest response time) and highest gains are observed near the trailing edge of the wing**,** close to the location of the actuator. Interestingly, all responses exhibit a very simple first order dynamics. These step responses are thus identified as first order ones with variable gains and response times depending on the location around the chord. In order to have an overview of the multiple outputs of the system, we fitted the following first order response type for each pressure tap :

$$P(t) - P_i = Ku(t)(1 - e^{-\frac{t}{\tau}}), \tag{3}$$

where P is the pressure, t the time, K the steady state gain, τ the time constant of the system (i.e. time to reach 63% of the steady state), P_i the initial value of the pressure over the upper surface of the blade and $u(t)$ is the control input that is equal to unity when actuation is ON. Typical fitted results are plotted over the measured data points in figure 6. Note that a small constant time delay of $\Delta t^* = 0.46$, expres-

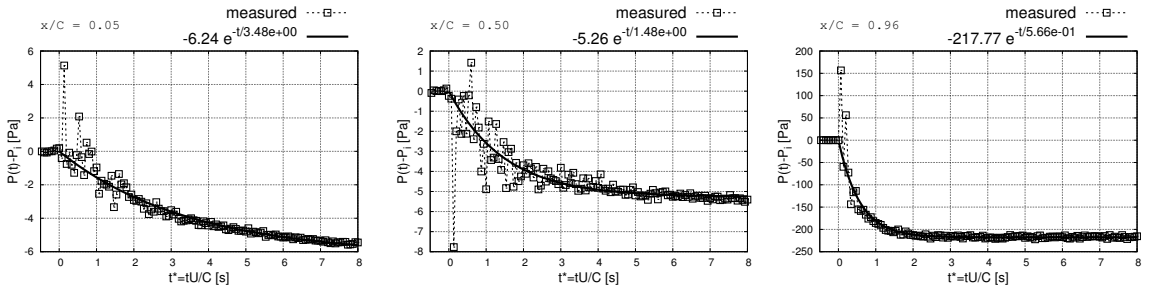

FIGURE 6 – Pressure step response to actuation at several chord positions on the upper side of the wing ($C_\mu = 0.139$).

sed in convective time units, corresponding to the electronic and valve opening delay, has been removed from all the pressure responses. We plot in figure 7 (Left) the different dimensionless steady state gains found chordwise for different control inputs (i.e. C_μ). Results show that a significant peak of the gain is present near the location of the actuation but limited to its very close neighborhood. In another hand, a non negligible gain is present all chordwise. It is found that the respective contributions of both areas (i.e. nearby the actuation and around the chord) to the integrated gain (lift coefficient) are of the same order of magnitude. Therefore, these results show that the actuation used in this study, although very local, modifies the overall pressure field around the wing, similarly as can be found in other circulation control configurations.

Figure 7 (Right) show the dimensionless time constants τ found around the chord of the profile for different control inputs. The response time needed to reach 63% of the steady state range from 0.5 to 3.5 convective times. To reach 99% of the steady state, the chordwise response times range from 1.5 to 10.5 convective times. In the literature, for stalled wing (Colonius and Williams, 2011; Williams et al., 2009) and detached flow (Mathis et al., 2009; Shaqarin et al., 2013) configurations, only one value of the response time is given and measured either through one output global (lift) or local quantity (pressure, friction probe), corresponding to the largest response time found in the present study, $\tau U/C = 10$.

The present study shows a clear evidence that the response of the system gets slower as the distance from the actuation increases. This indicates that the chordwise pressure distribution at a time shorter than the largest time constant to reach the steady state (i.e. transient lift), is associated with the creation of pitch torque.

Also, contrary to what is reported by many authors (Darabi and Wygnanski, 2004a,b; Mathis et al., 2009), we didn't find significant differences between dynamic responses to an actuation step ON (open symbols of figure 7) and an actuation step OFF (closed symbols of figure 7). The main difference between studies is the initial state of the flow before control. In the present study the flow is attached all the time while in the other studies the flow is either initially separated (Darabi and Wygnanski, 2004a,b), or the final targeted state is the flow separation (Mathis et al., 2009). This suggests that theses differences have to be attributed to the dynamic of the separated flow itself.

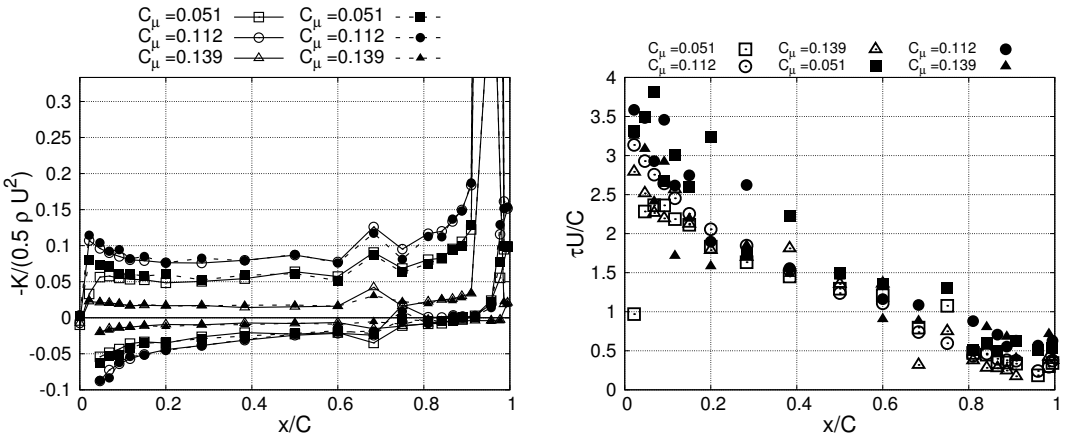

FIGURE 7 – Left : chordwise evolution of the gains K for varying actuation intensities, the vertical axis was chose to cut-off the very high gains obtained in the neighborhood of the actuator, open and closed symbols are for opening and closing actuation respectively. Right : chordwise evolution of the time responses τ for varying actuation intensity.

4.2 Lift coefficient

From the former phase locked pressure step responses, it is possible to build the corresponding lift step responses by simply integrating the pressure field on the wing surface :

$$C_L(t) \quad = \quad \frac{1}{S_{ref}} \int_S C_p(\mathbf{x}, t) d\mathbf{x} \tag{4}$$

where $C_p(\mathbf{x}, t) = \frac{P(\mathbf{x},t)-P_\infty}{0.5\rho U_\infty}$ the pressure coefficient with $\mathbf{x}$ the projection of the chord coordinates on the streamwise direction.

The obtained lift step response is plotted in figure 8 for the three different momentum coefficients investigated here. If the lift gain is normalized by the steady state gain, all the lift responses collapse onto a single curve corresponding to a typical step response from a first order system. A least-square approximation of $C_L(t)$ is obtained by fitting a $1-e^{t/\tau}$ function with the experimental data. The result is plotted against experimental measurement points in figure 8. The response time to reach 63% of the steady state is found very close to one convective time $\tau = \frac{C}{U}$ which means that the time to reach 99% of the steady state is 3 convective times.

This time response is more than 3 times faster than what has been previously observed in stalled configurations who reported a system response time of about 10 convective times Colonius and Williams (2011) and Williams et al. (2009).

This response time scale has to be compared with the times scales of perturbations that can be found in the atmospheric boundary layer. Typical spectrum of atmospheric boundary layer velocity fluctuations are given in figure 9, based on the formula given by Kaimal et al. (1972). This spectrum is plotted against a reduced frequency representative of the characteristic scales of an existing wind turbine blade with chord length of 1m and velocity of 60m/s. As can be seen, most of the velocity perturbations are low frequency with respect to the blade time scales : the peak frequency of all the perturbations are found below $St < 0.1$ for all the 3 velocity components. Since the open-loop control system has a characteristic frequency of $St = 1$, it is clear that the proposed system is rapid enough to account for those scales. This is illustrated in figure 9, where the shaded area corresponds to frequencies above the cut-off

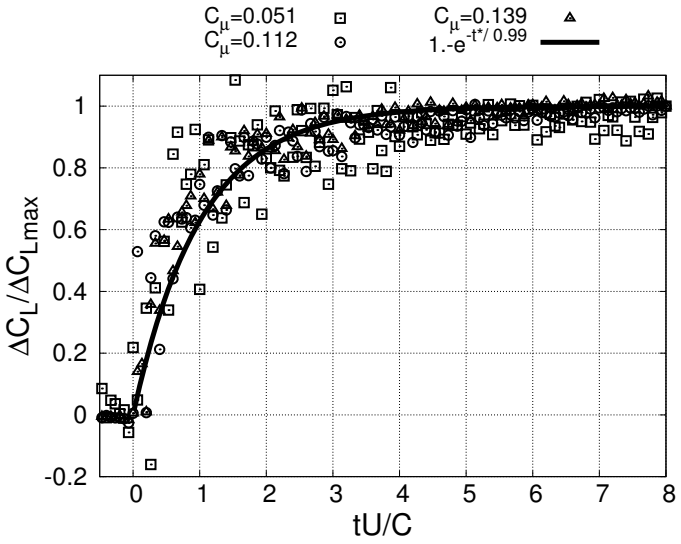

FIGURE 8 – Step response of the lift coefficient C_L obtained by integrating all the measured pressure responses.

frequency of the open-loop system, and the transfer function is presented in dark-grey.

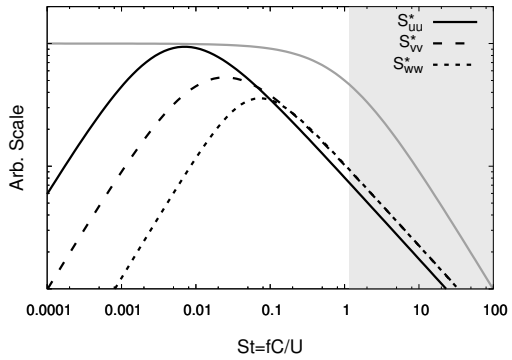

FIGURE 9 – Spectrum velocity perturbations in an atmospheric boundary layer taken at an altitude of $z = 80$m and average velocity of $8m/s$. The frequency is reduced by a wind turbine blade length and velocity scales. The grey curve represents the efficiency of the open-loop control system : beyond $St = 1$ the control system becomes inefficient.

5 Conclusions

An experiment was designed to evaluate the lift dynamics of a pre-stalled wind-turbine blade using control of circulation at its trailing-edge. The chosen blade profile is a modified $NACA - 65_4421$. The control is performed by means of a spanwise line of squared fluidic micro-jets located just before the rounded trailing-edge. The control of aerodynamic performances were validated through lift and drag measurements. Steady results shows that the proposed control is able to linearly increase lift of the profile, with an increasing efficiency with angle of attack. Then, chordwise investigations of the dynamics was performed through unsteady pressure measurements and analysis of responses to steps in actuation. All identified dynamics were found to be of the first order kind with time responses and a steady state gains that depend on the distance to the actuation. This chordwise arrangement of response times create

a transient pitch torque during the control action that should be accounted for if this system is to be integrated. Finally, the dynamics of the lift coefficient was investigated through integration of pressure measurements. The universal first order response of the system for stalled or separated configurations in the literature is here extended to pre-stalled configurations, but with a response time approximately 3 times faster. This indicates that the dynamics associated to a flow separation or reattachement differs greatly than the lift dynamics of a pre-stalled wing.

6 Acknowledgements

The authors wish to thank the PRISME Laboratory staff for their help conducting the experiments. The authors also wish to thank the support of the French National Research Agency through the SMARTEOLE project (ANR-14-CE05-0034).

Références

S. Baleriola, A. Leroy, S. Loyer, P. Devinant, and S. Aubrun. Circulation control on a rounded trailing-edge wind turbine airfoil using plasma actuators. In *Journal of Physics : Conference Series*, volume 753, page 052001. IOP Publishing, 2016.

C. Braud and E. Guilmineau. Jet flow control at the blade scale to manipulate lift. In *Journal of Physics : Conference Series*, volume 753, page 022031. IOP Publishing, 2016.

C. M. Cagle and G. S. Jones. A wind tunnel model to explore unsteady circulation control for general aviation applications. In *22nd AIAA Aerodynamic Measurement Technology and Ground Testing Conference*, pages 24–26, 2002.

T. Colonius and D. R. Williams. Control of vortex shedding on two-and three-dimensional aerofoils. *Philosophical Transactions of the Royal Society of London A : Mathematical, Physical and Engineering Sciences*, 369(1940) :1525–1539, 2011.

A. Darabi and I. Wygnanski. Active management of naturally separated flow over a solid surface. part 1. the forced reattachment process. *Journal of Fluid Mechanics*, 510 :105–129, 2004a.

A. Darabi and I. Wygnanski. Active management of naturally separated flow over a solid surface. part 2. the separation process. *Journal of Fluid Mechanics*, 510 :131–144, 2004b.

A. Dumitrache, F. Frunzulică, H. Dumitrescu, R. Mahu, and S. Sivasundaram. Active and passive circulation control as enhancement techniques of wind turbines performance. In *AIP Conference Proceedings*, volume 1493, pages 330–337. AIP, 2012.

R. J. Englar. Two-dimensional subsonic wind tunnel tests on a cambered 30 percent-thick circulation control airfoil. *Naval Ship Research and Development Center. Tech. Note AL-201)(In preparation) ii*, 1972.

R. J. Englar. Experimental investigation of the high velocity coanda wall jet applied to bluff trailing edge circulation control airfoils. Technical report, DTIC Document, 1975.

R. J. Englar and R. M. Williams. Design of a circulation control stern plane for submarine applications. Technical report, DTIC Document, 1971.

G. S. Jones, S. A. Viken, A. E. Washburn, L. N. Jenkins, and C. M. Cagle. An active flow circulation controlled flap concept for general aviation aircraft applications. *AIAA paper*, 3157(1), 2002.

M. Kadosch. Déviation des jets par adhérence à une paroi convexe. *Journal de Physique Appliquée*, 19 (S4) :1–12, 1958.

J. Kaimal, J. Wyngaard, Y. Izumi, and O. Coté. Spectral characteristics of surface-layer turbulence. *Quarterly Journal of the Royal Meteorological Society*, 98(417) :563–589, 1972.

J. Kweder, C. C. Panther, and J. E. Smith. Applications of circulation control, yesterday and today. *International Journal of Engineering*, 4(5) :411, 2010.

A. Leroy, C. Braud, S. Baleriola, S. Loyer, P. Devinant, and S. Aubrun. Comparison of flow modification induced by plasma and fluidic jet actuators dedicated to circulation control around wind turbine airfoils. In *Journal of Physics : Conference Series*, volume 753, page 022012. IOP Publishing, 2016.

R. Mathis, A. Lebedev, E. Collin, J. Delville, and J.-P. Bonnet. Experimental study of transient forced turbulent separation and reattachment on a bevelled trailing edge. *Experiments in Fluids*, 46(1) : 131–146, 2009.

A. Seifert, T. Bachar, D. Koss, M. Shepshelovich, and I. Wygnanskil. Oscillatory blowing : a tool to delay boundary-layer separation. *AIAA journal*, 31(11) :2052–2060, 1993.

T. Shaqarin, C. Braud, S. Coudert, and M. Stanislas. Open and closed-loop experiments to identify the separated flow dynamics of a thick turbulent boundary layer. *Experiments in fluids*, 54(2) :1448, 2013.

A. Shires and V. Kourkoulis. Application of circulation controlled blades for vertical axis wind turbines. *Energies*, 6(8) :3744–3763, 2013.

V. Troshin and A. Seifert. Performance recovery of a thick turbulent airfoil using a distributed closed-loop flow control system. *Experiments in fluids*, 54(1) :1443, 2013.

D. Williams, W. Kerstens, S. Buntain, V. Quach, J. Pfeiffer, R. King, G. Tadmor, and T. Colonius. Closed-loop control of a wing in an unsteady flow. *AIAA Paper*, pages 2010–0358, 2010.

D. R. Williams, G. Tadmor, T. Colonius, W. Kerstens, V. Quach, and S. Buntain. Lift response of a stalled wing to pulsatile disturbances. *AIAA journal*, 47(12) :3031–3037, 2009.

G. Woo, T. Crittenden, and A. Glezer. Transitory control of a pitching airfoil using pulse combustion actuation. In *4th Flow Control Conference*, page 4324, 2008.